NOTES AND CORRESPONDENCE

An Experiment on the Nonbreaking Surface-Wave-Induced Vertical Mixing

DEJUN DAI AND FANGLI QIAO

First Institute of Oceanography, State Oceanic Administration, Qingdao, China

WOJCIECH SULISZ

Institute of Hydroengineering, Polish Academy of Sciences, Gdańsk, Poland

LEI HAN

First Institute of Oceanography, State Oceanic Administration, Qingdao, China

ALEXANDER BABANIN

Swinburne University of Technology, Melbourne, Victoria, Australia

(Manuscript received 2 October 2009, in final form 27 April 2010)

ABSTRACT

Mixing induced by nonbreaking surface waves was investigated in a wave tank by measuring the thermal destratification rate of the water column. One experiment without waves and four experiments with waves of amplitudes ranging from 1.0 to 1.5 cm and wavelength from 30 to 75 cm were conducted. Water temperature variations at depths from 4 to 12 cm below the surface were measured. In the layer from 4 to 7 cm, the originally dense isothermal lines disperse soon after the waves are generated, whereas the vertical gradient from 9 to 12 cm is maintained for a relatively long time. The time span, during which the water temperature becomes well mixed, changes from about 20 h for the case with no waves to tens of minutes for the case with waves, and it decreases with increasing wave amplitude and wavelength. A one-dimensional diffusion numerical model with wave-induced mixing parameterization shows consistent results with the measurement. The study demonstrates that the mixing induced by nonbreaking waves may add an important contribution to the vertical mixing process in the upper ocean and suggests a way to parameterize wave-induced mixing in numerical ocean models.

1. Introduction

Energy input from wind to the surface waves, integrated over the World Ocean, is about 60 TW (Wang and Huang 2004). Such a large amount of energy will dissipate and cause mixing in the ocean mixed layer. Qiao et al. (2004) proposed a parameterization scheme for the nonbreaking surface-wave-induced vertical mixing (NBWAIM), and numerical experiments show that this parameterization can significantly improve the performance of the ocean circulation models (Qiao et al. 2004; Xia et al. 2006) and climate models (Song et al. 2007; Huang et al. 2008; Babanin et al. 2009). Although field observations suggest that surface waves can generate vertical mixing (e.g., Matsuno et al. 2006), it is still difficult to distinguish the mixing originated from breaking and nonbreaking process. Babanin (2006) suggested the same idea that the wave orbital motion can directly generate turbulence without breaking when the wave-amplitude-based Reynolds number is above the critical value: that is, $Re_{cr} \approx 3000$. The existence of wave-induced turbulence was verified by Babanin and Haus (2009) through laboratory experiment with monochromatic nonbreaking waves.

Effects that surface waves impose on mixing in the upper-ocean layer have been investigated in a number of different ways. First, wave breaking can generate turbulence and then leads to mixing in the upper-ocean

Corresponding author address: Fangli Qiao, Key Laboratory of Marine Science and Numerical Modeling, First Institute of Oceanography, 6 Xianxialing Road, Qingdao 266061, China.
E-mail: qiaofl@fio.org.cn

DOI: 10.1175/2010JPO4378.1

layer (Weber 2008). The direct mixing effects of wave breaking, however, are mainly limited within the layer of the order of the wave height or even shallower (Rapp and Melville 1990; Kantha and Clayson 2004; Noh and Min 2004; Gemmrich 2010), and existing schemes of diffusion of the surface-breaking turbulence down to the bottom of the mixed layer may have serious physical problems (e.g., Babanin et al. 2009).

In this regard, vertical advection of the surface turbulence by Langmuir circulation is a much more plausible mechanism (e.g., Melville et al. 1998). Indeed, the surface waves and wind are responsible for the generation of Langmuir circulation (Craik 1977; Phillips 2003; Sullivan and McWilliams 2010), which has the capability to transport downward turbulent kinetic energy generated by wave breaking or other processes at the sea surface, and they can also transfer some of their kinetic energy directly into turbulence (Kantha and Clayson 2004; Kukulka et al. 2009).

Finally, surface waves can also transfer energy into turbulence without breaking (Kitaigorodskii et al. 1983). Cheung and Street (1988) mentioned that, in the wind-ruffled mechanically generated wave cases, kinetic energy is transferred from the wave field to the mean flow by the wave-induced Reynolds stress and in turn is transferred to turbulence by turbulent viscosity. Jiang et al. (1990) suggested a significant energy exchange among the mean, wave-induced, and turbulent flow fields, which was then validated by field experiments (Anis and Moum 1995). Thais and Magnaudet (1996) studied the wave–turbulence interactions in a large wave channel and found that the turbulence was deeply affected by the wave motion. Ardhuin and Jenkins (2006) pointed out that the interaction of the wave-caused Stokes drift with ocean turbulence accounts for some fraction of the energy losses of the wave field in the ocean. All these mechanisms describe the interactions of waves with preexisting background turbulence.

Here, we will attempt to investigate turbulence directly induced by the waves in absence of wave breaking and other turbulence sources. Considering that mixing process can lead not only to the momentum but also to the heat transfer (Gemmrich and Farmer 1999; Gemmrich 2000), it is reasonable to estimate mixing by measuring variations of the water temperature rather than directly measuring the microscale velocity as had been done by Anis and Moum (1995) and Babanin and Haus (2009).

2. Experimental design

The experiments were carried out in a wave tank at the First Institute of Oceanography, State Oceanic Administration, Qingdao, China. The wave tank is 5 m long, 0.4 m high, and 0.3 m wide (Fig. 1). Refrigeration tubes are installed at the tank bottom to cool the water. The tank is equipped with a dissipation beach at one end and a piston mechanical wavemaker at the other end. Generally, the initial velocity profile generated by the wavemaker is different from typical surface waves. However, the nonpotential disturbances cannot propagate down the tank. The waves will readjust the velocity profile into a vertically decayed wave-induced flow within a few wavelengths (Babanin 2009); thus, away from the wavemaker, the waves' behavior is similar to that of surface ocean waves in the ocean. For insurance, an acoustic Doppler velocimeter is used to measure the horizontal and vertical velocities induced by surface waves with an amplitude of 1.0 cm and a wavelength of 75 cm at the center of wave channel: that is, 2.5 m away from the wavemaker. Both the horizontal and vertical velocity magnitudes and their decaying behavior are quite close to theoretical results (figures not shown).

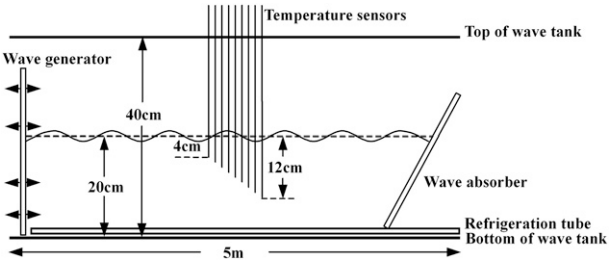

FIG. 1. The laboratory setup.

Needles of temperature sensors (Pt 100) with a 0.1-cm diameter and a 0.1-K resolution are used to automatically record the water temperature variation with a 1.0-Hz sampling frequency. The sensors are installed in the center of the wave channel: that is, 2.5 m away from wave generator and far away from all boundary layers. Nine sensors with a 1.0-cm vertical interval are arranged at the water depths of 4–12 cm (Fig. 1). A ruler is vertically affixed outside the glass wall of the wave tank, and pictures are taken to calculate the wave height when waves are generated. The wave period is obtained by a stopwatch, which measures the time span for 50 waves. The wavelength is calculated from the dispersion relation for the surface waves.

In all the laboratory experiments, the water depth in the channel is 20 cm. For each experiment, we first refrigerated the water for about 20 min through the bottom-mounted refrigerating tubes and then turned off the power. By this time, the water temperature at the 4-cm depth remains almost unchanged while ice appears at the bottom of the wave tank, because the refrigerating rate rather than the temperature of the tubes is kept unchanged for the refrigerating system. About one and

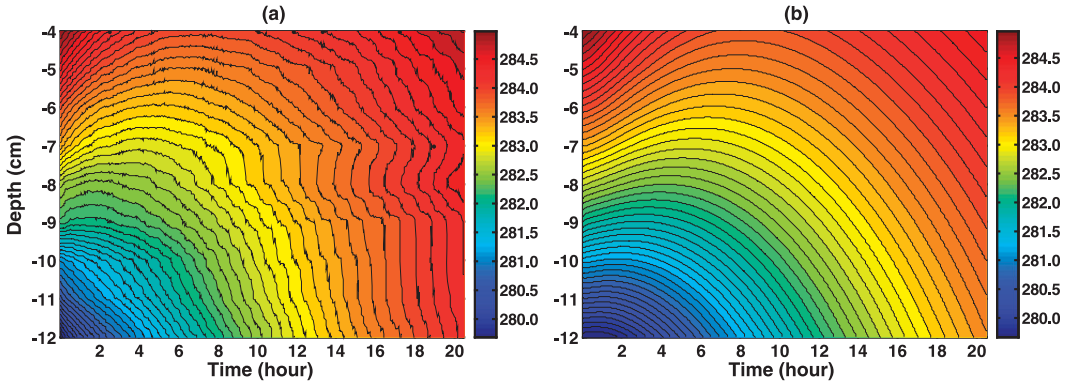

FIG. 2. Evolution of the water temperature profile without waves: (a) observations and (b) numerical simulation with the one-dimensional model. The time is in hours.

a half hours later, the ice is completely melted away and the generally steady temperature gradient is established. The temperature difference between the depths of 4 and 12 cm (TD4_12) was about 5 K. Then, monochromatic waves are generated until TD4_12 drops to 0.1 K. The temperature data are then used to analyze the influence of surface waves on the water temperature profile.

3. Experiment results

One experiment without waves and four experiments with different wave amplitudes and periods were conducted. For all four experiments with waves, there was no wave breaking.

Figure 2a illustrates the observed evolution of the temperature profile without waves. The starting time is chosen as a moment when the ice at the bottom melts away, and the water temperature is generally steadily stratified with apparent vertical gradient. The slow destratification process is clearly seen in the figure. The density of the isothermal lines changes from being compressed at the beginning to expanded at the end of the experiment. It takes about 20.5 h during which TD4_12 reduces from 5.0 to 0.6 K. The temperature at 4 cm decreases from 285.0 K at the beginning to 284.0 K about 7 h later and then increases to 284.9 K at the end of the experiment. Therefore, even after over 20 h, the molecular diffusion is insufficient to completely mix the top 12 cm of the water column. The interim warming at 4 cm is attributed to the surface heat transfer from the air above the water, because the air temperature is about 287 K, which is higher than the water temperature. Figure 2b shows results of a one-dimensional diffusion numerical model with molecular diffusivity $k = 1.4 \times 10^{-7}$ m^2 s^{-1} (see details of the diffusion model in section 4). The simulated behavior of the temperature variation is qualitatively and quantitatively similar to the observed. It suggests that the observed temperature variations with no waves are indeed controlled by molecular diffusion.

Four experiments with waves of different amplitudes and wavelengths (wave period) ranging from 30 cm (0.44 s) to 75 cm (0.72 s) are conducted to check whether there is NBWAIM and to study its dependence on wave characteristics. The results are shown in the left panels of Fig. 3. The initial time of each figure corresponds to the moment when the waves are just generated after the steady temperature stratification with the TD4_12 of about 5.0 K was set up.

Figures 3a,c,e show temperature variations with the fixed wave amplitude of 1.0 cm and different wavelengths of 30, 52, and 75 cm, respectively. Figures 4a,c,e offer the expanded first 40, 25, and 25 min for the three cases. For a wave amplitude of 1.0 cm and a wavelength of 30 cm, isothermal lines in the layer from 4 to 8 cm go from being compressed to being expanded, within several minutes after the waves are generated, whereas the dense isothermal lines in the layer from 9 to 12 cm remain compressed for a relatively long time. The upper mixed layer gradually deepens, and the dense isothermal lines in the layer from 9 to 12 cm eventually disappear. At 70 min after the waves are generated, the water temperatures from 4 to 12 cm are almost well mixed. At about 80 min, the TD4_12 drops to 0.1 K. During the 3–8-min period, there is an interim temperature warming in the layer from 4 to 8 cm, which is attributed to the heat flux from the upper layers due to mixing. For wavelength of 52 and 75 cm, observed temperature variations show behaviors similar to the case with a 30-cm wavelength, but it takes about 50 min for the TD4_12 to drop to 0.1 K.

Figures 3g and 4g show results for wave amplitude of 1.5 cm and wavelength of 75 cm. In this case, the isothermal lines in the layer from 4 to 7 cm become expanded

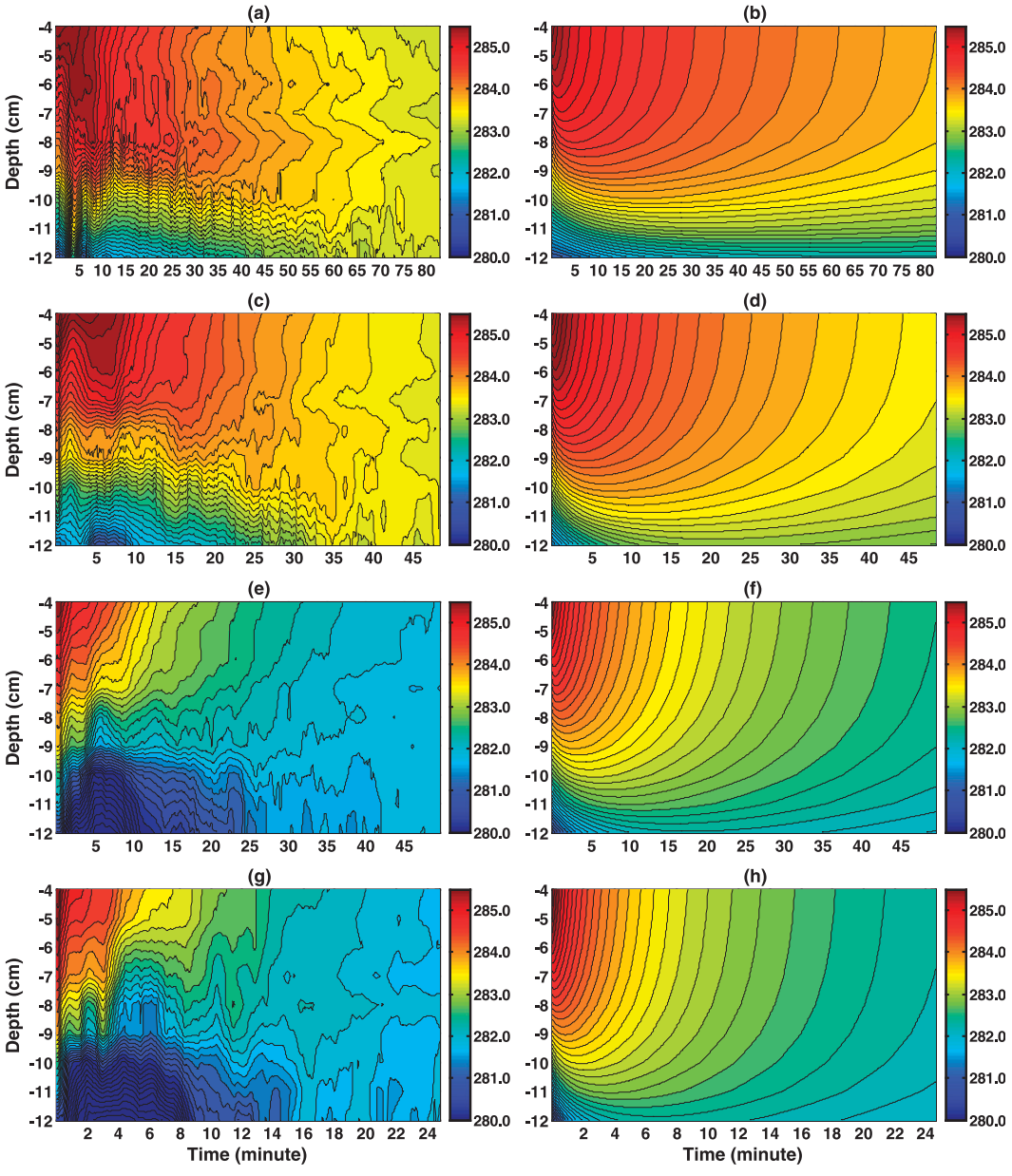

FIG. 3. (left) Evolution of the observed temperature profiles in four experiments with nonbreaking waves and (right) simulation results by means of the one-dimensional diffusion model: (a),(b) wave amplitude of 1.0 cm and wavelength of 30 cm; (c),(d) wave amplitude of 1.0 cm and wavelength of 52 cm; (e),(f) wave amplitude of 1.0 cm and wavelength of 75 cm; and (g),(h) wave amplitude of 1.5 cm and wavelength of 75 cm. The time is in minutes.

soon after the waves are generated. The dense isothermal lines persist for a relatively long time and gradually disappear, which indicates that the mixed layer deepens with time. About 24 min after the waves are generated, the water column from 4 to 12 cm is well mixed and the TD4_12 drops to 0.1 K.

Compared with the results without waves (Fig. 2), the four experiments with waves (Figs. 3, 4) clearly show the strong impact of surface waves on the water temperature through the additional wave-induced mixing. In summary, two characteristics can be found in the four experiments with waves. First, the isothermal lines in the layer from 4 to 7 cm are expanded while the lines in the layer from 9 to 12 cm remain compressed soon after the waves are generated. Second, the upper mixed layer gradually deepens, and the dense isothermal lines in the lower layer eventually disappear. These two characteristics suggest that the NBWAIM will be larger in the

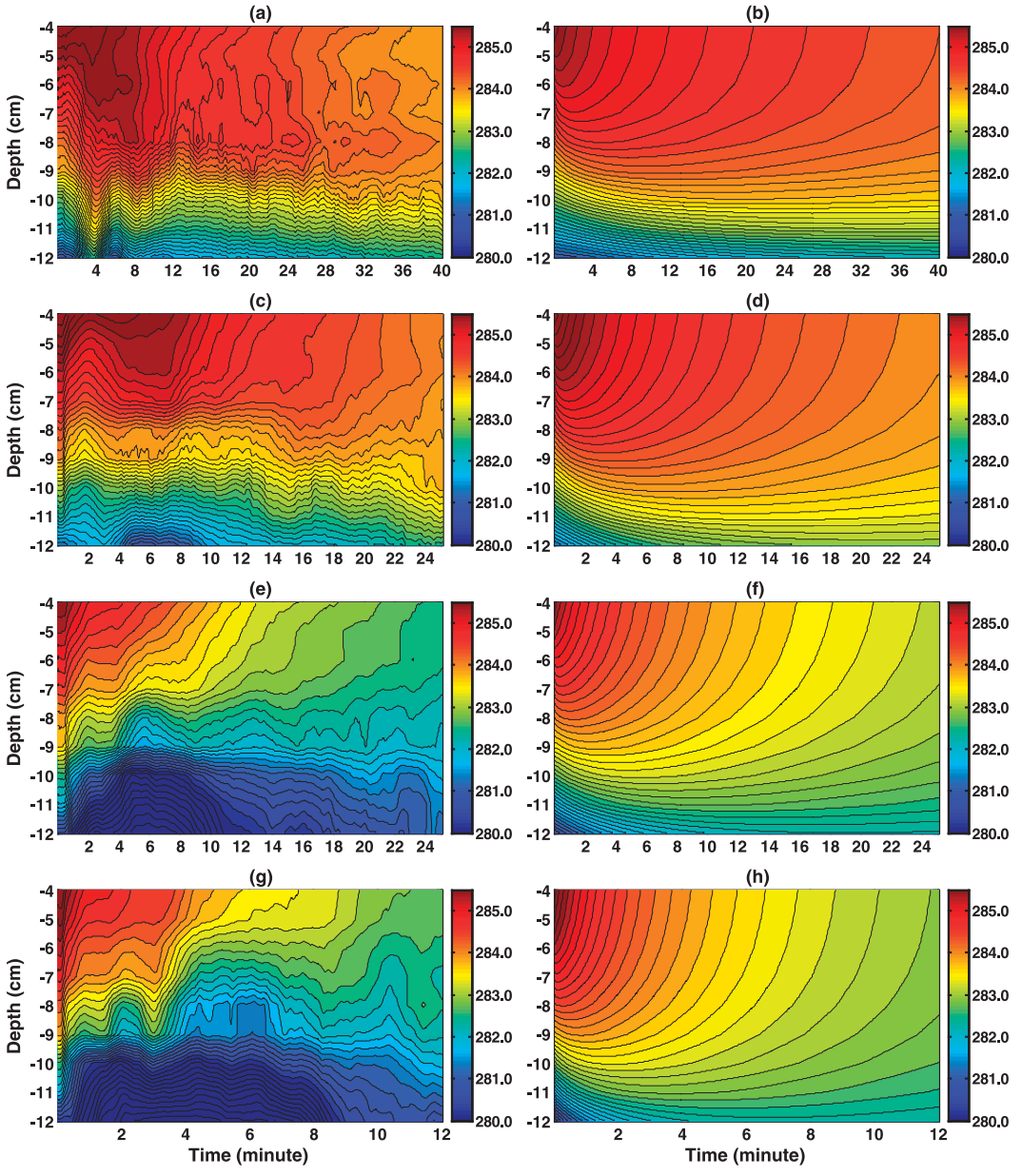

FIG. 4. As in Fig. 3, but for an expanded axis for the first 40, 25, 25, and 12 min of the four cases.

upper layer and smaller in the lower layer. In fact, this fact is consistent with the way the NBWAIM should work, considering the decay with depth of the orbital velocity of surface gravity waves, as suggested by Qiao et al. (2004), Babanin (2006), and Babanin and Haus (2009). Moreover, the orbital velocity is proportional to wave amplitude, and the decaying rate is inverse proportional to wavelength. It implies that the mixing time may be longer for small-amplitude waves and shorter for large-amplitude waves when the wavelength is fixed; similarly, the mixing time is longer for small wavelengths and shorter for large wavelengths when the wave amplitude is fixed. Our experimental results thus qualitatively agree with the theoretical orbital wave motion. When the wavelength is 75 cm, the period, during which the water temperature between 4 and 12 cm becomes well mixed (i.e., the TD4_12 drops from about 5.0 K at the beginning to 0.1 K at the end), decreases from 50 min for a wave amplitude of 1.0 cm (Fig. 3e) to about 24 min for a wave amplitude of 1.5 cm (Fig. 3g). On the other hand, for the wave amplitude of 1.0 cm, the mixing time reduces from 80 min for a wavelength

of 30 cm (Fig. 3a) to 50 min for a wavelength of 52 cm (Fig. 3c).

4. One-dimensional temperature diffusion model

In this section, a one-dimensional temperature diffusion model will be used to explain the observed phenomena. The governing equation for temperature diffusion can be expressed as

$$\frac{\partial T}{\partial t} = \frac{\partial}{\partial z}\left(k_z \frac{\partial T}{\partial z}\right), \tag{1}$$

where T is the water temperature, k_z is the vertical diffusion coefficient, t is the time, and z is the vertical coordinate (positive upward); $k_z = k_b + B_v$, where B_v represents the NBWAIM and k_b ($=1.4 \times 10^{-7}$ m^2 s^{-1}) is the background molecular diffusivity. Under an assumption of no wave breaking, Qiao et al. (2004) provided a parameterization scheme for surface-wave-induced turbulent-diffusion mixing, and its application to the numerical models has shown that the parameterization can significantly improve the simulation results of the upper mixed layer (Qiao et al. 2004, 2010; Xia et al. 2006). Then the NBWAIM, provided by Qiao et al. (2004, 2010), was selected as B_v after being extended to finite-depth environments.

From Eq. (9) in Qiao et al. (2004), we have

$$B_v = \overline{l_w w_w'}, \tag{2}$$

where l_w is mixing length of the wave-induced turbulence, which is proportional to the range of the wave particle displacement, and w_w' is the wave-induced vertical velocity fluctuation within the mixing length, which can be expressed as

$$w_w' = l_w \frac{\partial \sqrt{\overline{w_w w_w}}}{\partial z}. \tag{3}$$

Then, substituting the solutions for surface waves in the shallow water,

$$\begin{aligned} l_w &\propto \mathrm{Re}\left\{A \frac{\sinh k(z+d)}{\sinh kd} \exp[i(kx - \omega t)]\right\} \\ w_w &= \mathrm{Re}\left\{-iA\omega \frac{\sinh k(z+d)}{\sinh kd} \exp[i(kx - \omega t)]\right\}, \end{aligned} \tag{4}$$

into Eqs. (2) and (3) yields

$$B_v = \alpha A^3 k \omega \left[\frac{\sinh k(z+d)}{\sinh kd}\right]^3, \tag{5}$$

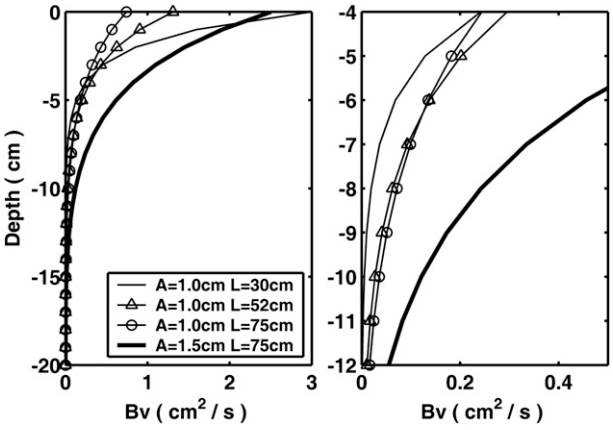

FIG. 5. The B_v profiles used in the one-dimensional model: (left) the entire depth of the experimental tank (0–20-cm depth) and (right) the depths of the temperature measurements (4–12-cm depth).

where A is wave amplitude, k is wavenumber, ω is frequency, d is the water depth, α is a constant, and we set $\alpha = 1$ in this study as in Qiao et al. (2004). Equation (5) shows that B_v is proportional to the cubic amplitude, the frequency, and wavenumber while it decays with the water depth. The characteristics can be found in Fig. 5, which shows the B_v profiles of the four experiments described here.

The upper boundary condition is chosen as

$$k_z \frac{\partial T}{\partial z}\Big|_{z=0} = \frac{q}{\rho c}, \tag{6}$$

where q represents the heat flux (W m^{-2}) at the water surface, which includes the latent, sensible heat fluxes and the heat flux from environmental longwave radiation; ρ is the water density; and c is the specific heat capacity. Bulk formulas are used to estimate the latent and sensible heat fluxes (Stewart 2005), whereas the orbital velocities of surface waves are treated as the equivalent wind speeds at 1.0 cm above the water surface. The heat flux from the longwave radiation is estimated by the formula for blackbody radiation. In addition to the surface heat flux, longwave radiation will heat water through the side glass walls. For simplicity, we assume that the longwave radiation at any layer will homogeneously heat the horizontal layer of the water. Simulation results show that the surface heat flux is responsible for the observed temperature increase at 4 cm for experiments without waves. For experiments with waves, however, the surface and side heat fluxes are one order of magnitude smaller than the flux because of the turbulent diffusivity between neighboring layers so that the flux condition has little effect on the temperature

variations. For the bottom boundary, the no-flux condition is used,

$$\frac{\partial T}{\partial z}\Big|_{z=-d} = 0, \tag{7}$$

where $d = 20$ cm. The initial conditions are obtained by interpolating or extrapolating from the observations.

a. Results of numerical experiment without waves

To compare model results with the observed data, model outcomes between 4 and 12 cm from the surface are shown in Fig. 2b. One can see that the numerical outcome is very close to the observations. The mean absolute error of the simulated temperature variation is 0.15 K. Close examination shows that the vertical temperature gradient is dominated by the molecular diffusivity rather than the surface heat flux, which is only responsible for the observed temperature increase of the top 4 cm or so. As a sensitivity test, we also simulate the temperature variations with $k_b = 1.0 \times 10^{-8}$ m^2 s^{-1} and $k_b = 1.0 \times 10^{-6}$ m^2 s^{-1}, separated by an order of magnitude in each direction from the original molecular diffusion. As expected, the results are totally different from the observations (figures not shown). It implies that the temperature variation in absence of waves is indeed controlled by the molecular diffusivity. The excellent agreement between the model and observations also provides a strong support for the diffusion model employed in this study.

b. Results of numerical experiments with waves

The B_v profiles of the four wave experiments are shown in Fig. 5. The vertical distribution of B_v can qualitatively explain the observed mixing in our experiments. For a wave amplitude of 1.0 cm and a wavelength of 30 cm, B_v is the maximum near the surface but decays with depth faster than the other cases, so the mixing values are smaller below 4 cm than any of the other cases. The smallest mixing leads to the longest mixing time, as observed in our experiments. On the contrary, B_v decreases the slowest and becomes the largest for the 4–12-cm layer for wave amplitude of 1.5 cm and wavelength of 75 cm, leading to the shortest mixing time of the four cases. For the experiments with wavelengths of 52 and 75 cm (wave amplitude of 1.0 cm), B_v profiles at depths from 4 to 12 cm are similar. Both experiments require about 50 min to reach a mixed condition.

Numerical results with the additional wave mixing are shown in the right panel of Fig. 3. The expanded first 40, 25, 25, and 12 min are shown in the right panel of Fig. 4. From the simulated results, one can see that the initial isotherms in the layer from 4 to 7 cm are expanded and the lines in the layer from 9 to 12 cm are compressed. Moreover, the isothermal lines in the layer from 4 to 7 cm rapidly become vertical, which means that it takes only several minutes for the additional turbulent mixing described by B_v to make the temperature in the upper layer well mixed. During the further mixing, the isotherms below 7 cm become more and more expanded, indicating that temperatures in the entire 12 cm are actively mixed throughout the simulation period. These two features are observed in the laboratory experiments too, implying that the parameterization of the turbulent-diffusion coefficient B_v, whose source in the model is the surface waves alone, represents the wave-induced mixing quite well.

The origin of turbulence and the associated mixing is now further analyzed. In addition to the surface waves, internal waves may exist as well in our experiments because of the stratification. Observed temperature time series are analyzed to identify potential internal waves. The analysis shows that internal waves with periods between about 20 and 80 s are evident at the 95% confidence level. However, the Richardson numbers for these internal waves are much larger than 0.25, implying that the internal waves in the wave tank should not lead to production of turbulence and significant mixing.

Another potential mixing mechanism is due to shear associated with a return current that may occur in the wave tank. Generally, the return current should be driven by the Stokes drifts of the surface waves, which can be expressed as (Phillips 1977)

$$u_s = a^2 k\omega \frac{\cosh[2k(z+d)]}{2\sinh^2(kd)}. \tag{8}$$

The velocity of the return current will be much weaker than the Stokes drifts because of the existence of stratification. During the experiments, we used red ink as a tracer to detect the possible return current and found that the maximum velocity is smaller than 0.3 cm^{-1}, whereas the Stokes drifts at water surface calculated from Eq. (8) range from 0.8 to 3.0 cm^{-1}. The corresponding Reynolds number of shear current is as small as 500, which indicates that the shear current should not induce significant turbulent mixing. On the other hand, the heat transport by the return current will affect the temperature structure in the wave tank. However, it is believed that the corresponding effects on the destratification should be small compared with the surface-wave-induced mixing. For example, when a wave amplitude is 1.0 cm, the Stokes drift at the surface is largest (3.0 cm^{-1}) for a wavelength of 30 cm and smallest (0.8 cm^{-1}) for a wavelength of 75 cm. If the heat transport of the return

current is a dominant factor of the water temperature destratification, the mixing time for a wavelength of 75 cm should be longer than that for 30 cm, which is opposite to the observed results. Furthermore, the mixing time is about 20 min, the smallest time among our experiments, for a wave amplitude of 1.5 cm and a wavelength of 75 cm, but the Stokes drift at the surface is 1.8 cm^{-1}, neither the largest nor the smallest one. Therefore, the heat transport of the return current may affect the water temperature to some degree, but its impact is likely much smaller compared with the surface-wave-induced mixing.

In the absence of initial turbulence, as well as in the absence of wind forcing, shear currents, and noticeable internal waves and away from lateral boundaries, the observed turbulent mixing could have only been generated by the waves themselves. This is qualitatively consistent with other turbulent mixing models (Qiao et al. 2004, 2010) and observations (i.e., Babanin 2006; Babanin and Haus 2009). These results emphasize the need to improve existing ocean circulation models by including the surface-wave contribution to the upper-ocean mixing.

Despite the general good agreement between the model results and the water tank experiments, there are still some remaining discrepancies. For example, in the case with a wave amplitude of 1.0 cm and wavelength of 30 cm, the observed temperature of the 4–12-cm layer is well mixed within 80 min (Fig. 3a), whereas in the model some temperature gradients still exist in the 9–12-cm layer at this time (Fig. 3b). A similar pattern is seen in other experiments (Figs. 3c,d). Therefore, the model and the observed mixing characteristics are qualitatively similar, whereas the exact temperature values and spatial pattern may be slightly different. Note, for example, that the one-dimensional model results are smoother than the observations, because vertical mixing dominates in the model, whereas return currents and internal waves add more small-scale variations to the observed results. The impact of the return currents and internal waves on water temperature destratification needs further analysis and observations.

5. Discussion and summary

Babanin (2006) proposed a wave Reynolds number, $\mathrm{Re} = A^2\omega/\nu$, where ν is kinematic viscosity of the water, and suggested that the wave orbital motion can directly generate turbulence when the Reynolds number is above a critical number. Using the significant wave height, he estimated the critical number as $\mathrm{Re}_{cr} \approx 3000$ by assuming that all the mixing in the upper-ocean layer in April is done by the wave-induced turbulence. Babanin and Haus (2009) measured the wave-induced turbulence onset directly and found turbulent generation at Reynolds numbers as low as Re = 1300. This is consistent with the conclusion of Babanin (2006), because the turbulence observed by Babanin and Haus (2009) was highly intermittent and only persisted for a fraction of the wave period; therefore, a transition to fully turbulent wave motion should occur at higher Reynolds numbers.

In our experiment results shown in Fig. 3, the wave Reynolds numbers at the surface are 1250, 950, 780, and 1750, respectively. This is in reasonable agreement with the measurements of Babanin and Haus (2009), because even an intermittent turbulence would be sufficient to destratify the water over many wave periods.

In summary, five laboratory experiments, one without waves and four with different wave amplitudes and wavelengths, are conducted to study the NBWAIM by measuring water temperature variations. Observed results show that the water temperature reaches a homogenous state within tens of minutes in the presence of surface waves, whereas it takes more than 20 h without surface waves. The mixing rate increases with increasing either the wave amplitude or the wavelength. A one-dimensional diffusion model with the NBWAIM, B_v, introduced by Qiao et al. (2004, 2010) is set up for comparison with the laboratory observations. Numerical results generally reproduce the basic characteristics of the observed temperature variations. This supports the hypothesis that the observed phenomena can be explained by the surface-wave-induced mixing very well.

Acknowledgments. This study was supported by the National Natural Science Foundation of China through Grants 40730842, 40876015, and 40906017. AVB gratefully acknowledges financial support of the Australian Research Council through Grants LP0883888 and DP1093517 and Woodside Energy Ltd. through Grant LP0883888. It is highly appreciated that Professor Tal Ezer, Old Dominion University, helped to polish the English of this note. We are also indebted to Professor Shun Yu, First Institute of Oceanography, SOA, China, for assistance in laboratory experiments.

REFERENCES

Anis, A., and J. N. Moum, 1995: Surface wave–turbulence interactions: Scaling $\varepsilon(z)$ near the sea surface. *J. Phys. Oceanogr.,* **25,** 2025–2045.

Ardhuin, F., and A. D. Jenkins, 2006: On the interaction of surface waves and upper ocean turbulence. *J. Phys. Oceanogr.,* **36,** 551–557.

Babanin, A. V., 2006: On a wave-induced turbulence and a wave-mixed upper ocean layer. *Geophys. Res. Lett.,* **33,** L20605, doi:10.1029/2006GL027308.

——, 2009: Breaking of ocean surface waves. *Acta Phys. Slovaca,* **59,** 305–535.

——, and B. K. Haus, 2009: On the existence of water turbulence induced by nonbreaking surface waves. *J. Phys. Oceanogr.,* **39,** 2675–2679.

——, A. Ganopolski, and W. R. C. Phillips, 2009: Wave-induced upper-ocean mixing in a climate model of intermediate complexity. *Ocean Modell.,* **29,** 189–197.

Cheung, T. K., and R. L. Street, 1988: The turbulent layer in the water at an air-water interface. *J. Fluid Mech.,* **194,** 133–151.

Craik, A. D. D., 1977: The generation of Langmuir circulations by an instability mechanism. *J. Fluid Mech.,* **81,** 209–223.

Gemmrich, J. R., 2000: Temperature anomalies beneath breaking waves and the decay of wave-induced turbulence. *J. Geophys. Res.,* **105** (C4), 8727–8736.

——, 2010: Strong turbulence in the wave crest region. *J. Phys. Oceanogr.,* **40,** 583–595.

——, and D. M. Farmer, 1999: Near-surface turbulence and thermal structure in a wind-driven sea. *J. Phys. Oceanogr.,* **29,** 480–499.

Huang, C., F. Qiao, and Z. Song, 2008: The effect of the wave-induced mixing on the upper ocean temperature in a climate model. *Acta Oceanol. Sin.,* **27,** 104–111.

Jiang, J. Y., R. L. Street, and S. P. Klotz, 1990: A study of wave-turbulence interaction by use of a nonlinear water wave decomposition technique. *J. Geophys. Res.,* **95,** 16 037–16 054.

Kantha, L. H., and C. A. Clayson, 2004: On the effect of surface gravity waves on mixing in the oceanic mixed layer. *Ocean Modell.,* **6,** 101–124.

Kitaigorodskii, S. A., M. A. Donelan, J. L. Lumley, and E. A. Terray, 1983: Wave-turbulence interactions in the upper ocean. Part 2: Statistical characteristics of wave and turbulent components of the random velocity field in the marine surface layer. *J. Phys. Oceanogr.,* **13,** 1988–1999.

Kukulka, T., A. J. Plueddemann, J. H. Trowbridge, and P. P. Sullivan, 2009: Significance of Langmuir circulation in upper ocean mixing: Comparison of observations and simulations. *Geophys. Res. Lett.,* **36,** L10603, doi:10.1029/2009GL037620.

Matsuno, T., J.-S. Lee, M. Shimizu, S.-H. Kim, and I.-C. Pang, 2006: Measurements of the turbulent energy dissipation rate ε and an evaluation of the dispersion process of the Changjiang Diluted Water in the East China Sea. *J. Geophys. Res.,* **111,** C11S09, doi:10.1029/2005JC003196.

Melville, W. K., R. Shear, and F. Veron, 1998: Laboratory measurements of the generation and evolution of Langmuir circulations. *J. Fluid Mech.,* **364,** 31–58.

Noh, Y., and H. S. Min, 2004: Large eddy simulation of the ocean mixed layer: The effects of wave breaking and Langmuir circulation. *J. Phys. Oceanogr.,* **34,** 720–735.

Phillips, O. M., 1977: *The Dynamics of the Upper Ocean*. Cambridge University Press, 336 pp.

Phillips, W. R. C., 2003: Langmuir circulation. *Wind Over Waves II: Forecasting and Fundamentals of Applications,* S. G. Sajjadi and J. C. R. Hunt, Eds., Horwood, 157–167.

Qiao, F., Y. Yuan, Y. Yang, Q. Zheng, C. Xia, and J. Ma, 2004: Wave-induced mixing in the upper ocean: Distribution and application to a global ocean circulation model. *Geophys. Res. Lett.,* **31,** L11303, doi:10.1029/2004GL019824.

——, ——, T. Ezer, C. Xia, Y. Yang, X. Lü, and Z. Song, 2010: A three-dimensional surface wave-ocean circulation coupled model and its initial testing. *Ocean Dyn.,* in press, doi:10.1007/s10236-010-0326-y.

Rapp, R. J., and W. K. Melville, 1990: Laboratory measurements of deep-water breaking waves. *Philos. Trans. Roy. Soc. London,* **311A,** 735–800.

Song, Z., F. Qiao, Y. Yang, and Y. Yuan, 2007: An improvement of the too cold tongue in the tropical Pacific with the development of an ocean-wave-atmosphere coupled numerical model. *Prog. Nat. Sci.,* **17,** 576–583.

Stewart, R. H., cited 2005: Introduction to physical oceanography. Texas A&M University Dept. of Oceanography Open Source Textbook. [Available online at http://oceanworld.tamu.edu/resources/ocng_textbook/contents.html.]

Sullivan, P. P., and J. C. McWilliams, 2010: Dynamics of winds and currents coupled to surface waves. *Annu. Rev. Fluid Mech.,* **42,** 19–42.

Thais, L., and J. Magnaudet, 1996: Turbulent structure beneath surface gravity waves sheared by the wind. *J. Fluid Mech.,* **328,** 313–344.

Wang, W., and R. X. Huang, 2004: Wind energy input to the surface waves. *J. Phys. Oceanogr.,* **34,** 1276–1280.

Weber, J. E. H., 2008: A note on mixing due to surface wave breaking. *J. Geophys. Res.,* **113,** C11009, doi:10.1029/2008JC004758.

Xia, C., F. Qiao, Y. Yang, J. Ma, and Y. Yuan, 2006: Three-dimensional structure of the summertime circulation of the Yellow Sea from a wave-tide-circulation coupled model. *J. Geophys. Res.,* **111,** C11S03, doi:10.1029/2005JC003218.